Discovery of novel berberine imidazoles as safe antimicrobial agents by down regulating ROS generation

Si-Qi Wen, Ponmani Jeyakkumar, Srinivasa Rao Avula, Ling Zhang, Cheng-He Zhou

PII: S0960-894X(16)30446-2
DOI: http://dx.doi.org/10.1016/j.bmcl.2016.04.070
Reference: BMCL 23832

To appear in: *Bioorganic & Medicinal Chemistry Letters*

Received Date: 31 March 2016
Revised Date: 20 April 2016
Accepted Date: 23 April 2016

Please cite this article as: Wen, S-Q., Jeyakkumar, P., Avula, S.R., Zhang, L., Zhou, C-H., Discovery of novel berberine imidazoles as safe antimicrobial agents by down regulating ROS generation, *Bioorganic & Medicinal Chemistry Letters* (2016), doi: http://dx.doi.org/10.1016/j.bmcl.2016.04.070

Bioorganic & Medicinal Chemistry Letters
journal homepage: www.elsevier.com

Discovery of novel berberine imidazoles as safe antimicrobial agents by down regulating ROS generation

Si-Qi Wen, Ponmani Jeyakkumar[†], Srinivasa Rao Avula[‡], Ling Zhang, Cheng-He Zhou[*]

Institute of Bioorganic & Medicinal Chemistry, Key Laboratory of Applied Chemistry of Chongqing Municipality, School of Chemistry and Chemical Engineering, Southwest University, Chongqing 400715, PR China

ARTICLE INFO

Article history:
Received
Revised
Accepted
Available online

Keywords:
Berberine
Imidazole
Antimicrobial
ROS
DNA

ABSTRACT

A series of novel berberine-based imidazole derivatives as new type of antimicrobial agents were developed and characterized. Most of them gave good antibacterial activity towards the Gram-positive and negative bacteria. Noticeably, imidazolyl berberine **3a** exhibited low MIC value of 1 μg/mL against *E. typhosa*, which was even superior to reference drugs berberine, chloromycin and norfloxacin. The cell toxicity and ROS generation assay indicated that compound **3a** showed low cell toxicity. The interactive investigation by UV–vis spectroscopic method revealed that compound **3a** could effectively intercalate into calf thymus DNA to form **3a**–DNA complex which might further block DNA replication to exert the powerful antimicrobial activities. The binding behavior of compound **3a** to DNA topoisomerase IB revealed that hydrogen bonds and electrostatic interactions played important roles in the association of compound **3a** with DNA topoisomerase IB.

Microbial infection is a kind of commonly and frequently occurring infective disease worldwide. So far, a great number of antibiotics and synthetic drugs have been extensively used in clinic and have played a significant role in the treatment of microbial infections. However, along with the widespread use of antimicrobial drugs, the emergence of multidrug-resistant strains like methicillin-resistant *Staphylococcus aureus* (MRSA), *Staphylococcus epidermidis* (MRSE), vancomycin-resistant *Enterococccus faecium* (VRE) makes many traditional antibiotics and synthetic drugs decrease their effects or totally lose activities.[1] Therefore, the pursuit of structurally novel drugs with more efficiency, less toxicity and less resistance remains to be a highly challenging topic with much interest in medicinal chemistry.

Berberine (**1**, Fig. 1) is a well-known natural isoquinoline alkaloid from many kinds of medicinal plants such as *Hydrastis canadensis*, *Coptis rhizome*, *Coptis chinensis etc*. The alkaloid has been commonly used in the clinic to treat various diseases such as bacillary dysentery, acute gastroenteritis, cholera and other related diseases.[2] Its importantly clinical uses stimulate the continuing researches in antimicrobial field. Specially, literature revealed that berberine could exert antimicrobial effect not only by DNA breakage but also through accumulation of NorA substrate in bacterial cells.[3] Numerous efforts have been made to develop more effective berberine-based antimicrobial agents.[4] Our previous work showed that the introduction of heterocycles into C-9 position of berberine backbone could enhance the antimicrobial activities and broaden antimicrobial spectrum.[5] However, structural modification of the C-12 position in berberine backbone has been rarely reported.[6]

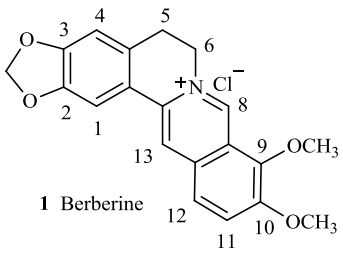

1 Berberine

Figure 1. Structure of berberine **1**.

Imidazole nuclus has been attracting increasing interest in drug design. The unique structure of imidazole ring is beneficial for its derivatives to readily interact with diverse biological molecules such as DNAs, enzymes and receptors in organism, thus exhibiting wide medicinal potentiality.[7] Meanwhile, the presence of imidazole ring may be favorable for improving water solubility to some extent. The introduction of imidazole has become an efficient approach for the natural product modification to improve bioactivity. Considering the potentiality of berberines in anti-infection field and as an extension of our studies on the development of azole compounds, herein we incorporated imidazole and its alkyl substituted derivatives into

* Corresponding author. Tel./fax: +86-23-68254967.
E-mail: zhouch@swu.edu.cn (C.-H. Zhou).
† PhD Candidate from India.
‡ Postdoctoral fellow from Medicinal and Process Chemistry Division, CSIR-Central Drug Research Institute, Lucknow 226001, India.

the C-12 position of berberine ring to develop a novel class of potential antimicrobial agents.

The synthetic route of berberine-derived imidazoles was outlined in Scheme 1. Berberrubine **2** could be efficiently prepared in yield of 88.4% by selective demethylation of berberine chloride **1** at 9-position heated at 190 °C under vacuum (20 mm Hg) for 30 minutes.[8] The obtained berberrubine **2** was further treated with imidazole and formaldehyde in dry n-butanol at 110 °C to produce the 12-substituted berberine imidazole derivatives **3a**–**j** in yield of 42–55%. It manifested that introduction of electron-withdrawing substituents including nitro or phenyl group on imidazole ring was unfavorable for the synthesis of target compounds. Moreover, the solvents and temperature also significantly affected the formation of products. Temperature less than 100 °C or changing the solvent all resulted in quite poor yield.

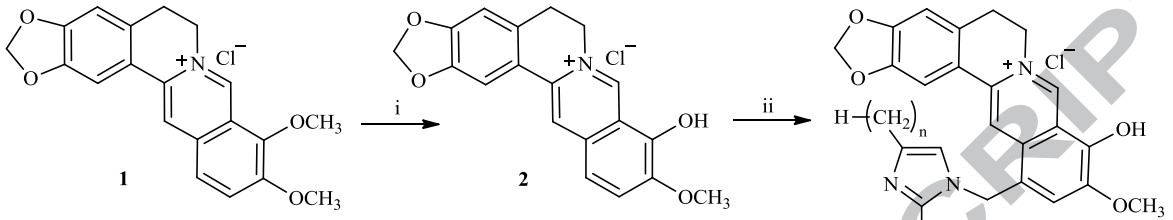

3a, m = 0, n = 0; **3b**, m = 1, n = 0; **3c**, m = 0, n = 1; **3d**, m = 2, n = 0; **3e**, m = 3, n = 0; **3f**, m = 4, n = 0; **3g**, m = 11, n = 0; **3h**, m = 17, n = 0; **3i**, m = 1, n = 1; **3j**, m = 2, n = 1

Scheme 1. Reagents and conditions: (i) 190 °C in vacuum (88.4% yield); (ii) imidazoles, formaldehyde aqueous solution (37%), hydrochloric acid (36%, catalytic amount), n-butanol (42–55% yield).

The newly synthesized compounds were evaluated for their antimicrobial activities *in vitro* against four Gram-positive bacteria (*S. aureus* ATCC25923, *S. aureus* N315, *B. subtilis* ATCC6633 and *M. luteus* ATCC4698), four Gram-negative bacteria (*E. coli* JM109, *P. aeruginosa* ATCC27853, *E. typhosa* ATCC14028 and *B. proteus* ATCC13315) as well as five fungi (*C. utilis* ATCC9950, *A. flavus* ATCC204304, *B. yeast*, ATCC9763, *C. albicans* ATCC10231, *C. mycoderma* ATCC9888) using the standard two folds serial dilution method in 96-well microtest plates according to the National Committee for Clinical Laboratory Standards (NCCLS).[9] Minimal inhibitory concentration (MIC, μg/mL) was defined as the lowest concentration of new compounds that completely inhibited the growth of microbes. Currently available antimicrobial drugs berberine, chloromycin, norfloxacin and fluconazole were used as the positive control. The values of ClogP were calculated using ChemDraw Ultra 10.0 software. The antibacterial and antifungal data as well as ClogP values were depicted in Table 1.

The antimicrobial activity showed that the new berberine-based imidazoles **3a**–**j** showed effective activities against all the tested bacteria and fungi with MIC values of 1–256 μg/mL, which were better than their precursor berberine. Excitingly, some prepared compounds were even more active than the reference drugs, especially better than chloromycin and norfloxacin. Particularly, compound **3a** showed excellent antimicrobial activities with broad antimicrobial spectrum in comparison with other compounds. Furthermore, the results also demonstrated that the imidazole fragment was important to exert excellent antimicrobial activity.

Table 1 *In vitro* antimicrobial data as MIC (μg/mL) for compounds **3a**–**j**[a,b,c,d]

Compds	ClogP	Gram-negative bacteria				Gram-positive bacteria				Fungi				
		E. coli	*B. proteus*	*P. aeruginosa*	*E. typhosa*	MRSA	*S. aureus*	*B. subtilis*	*M. luteus*	*C. utilis*	*A. flavus*	*B. yeast*	*C. albicans*	*C. mycoderma*
3a	-1.09	32	64	64	1	32	32	8	16	32	64	32	64	128
3b	-0.83	32	64	64	32	32	16	64	16	32	32	16	64	128
3c	-0.83	32	32	128	64	32	8	32	16	64	64	32	128	128
3d	-0.30	32	64	64	64	16	8	32	16	64	128	16	64	256
3e	0.23	64	64	128	64	32	16	64	32	128	128	32	64	128
3f	0.76	128	128	128	128	32	32	64	32	256	64	64	64	256
3g	4.46	256	128	256	256	64	128	128	128	256	256	128	128	128
3h	-	256	256	256	512	128	256	256	256	512	256	256	256	256
3i	-0.56	128	128	128	128	64	64	128	64	128	128	256	128	128
3j	-0.03	128	128	128	128	64	64	128	64	128	128	128	128	128
A	-0.77	512	256	256	512	128	512	512	512	256	512	128	512	128
B	-1.79	16	32	16	32	64	8	32	64	-	-	-	-	-
C	-0.78	16	4	2	4	8	2	1	2	-	-	-	-	-
D	-	-	-	-	-	-	-	-	-	8	256	16	32	32

[a] Minimum inhibitory concentrations were determined by micro broth dilution method for microdilution plates.
[b] **A** = Berberine, **B** = Chloromycin, **C** = Norfloxacin, **D** = Fluconazole.
[c] MRSA, Methicillin-Resistant *Staphylococcus aureus* N315; *S. aureus, Staphylococcus aureus* ATCC25923; *B. subtilis, Bacillus subtilis* ATCC6633; *M. luteus, Micrococcus luteus* ATCC4698; *E. coli, Escherichia coli* JM109; *P. aeruginosa, Pseudomonas aeruginosa* ATCC27853; *B. proteus, Bacillus proteus* ATCC13315; *E. typhosa, Eberthella typhosa* ATCC14028; *C. utilis, Candida utilis* ATCC9950; *A. flavus, Aspergillus flavus* ATCC204304; *B. yeast, Beer yeast* ATCC9763; *C. albicans, Candida albicans* ATCC10231; *C. mycoderma, Candida mycoderma* ATCC9888.
[d] ClogP values were calculated by ChemDraw Ultra 10.0.

Table 1 showed the obvious effects of the types of substituents on the imidazole ring on biological activity. Among all the berberine derivatives, compound **3a** gave the most potent antibacterial activity against *E. typhosa*, *B. subtilis* and MRSA with MIC values of 1–32 μg/mL, which was more active than chloromycin (MIC = 32–64 μg/mL) and berberine (MIC = 128–512 μg/mL). The introduction of alkyl substituted imidazole into 12-position of berberine yielded compounds **3b**–**j**, which

displayed weaker antibacterial activity than compound **3a** towards the tested strains. Only compounds **3c** and **3d** gave good anti-*S. aureus* with MIC value of 8 μg/mL, which was equivalent to chloromycin. These results suggested that the introduction of bulky alkyl group substituted imidazole fragment at C-12 position of berberine would decrease the antibacterial activity, possibly, the steric hindrance of the compounds makes it difficult to access the active site of validated target.

Specially, the *in vitro* antifungal evaluation revealed that the berberine-based 2-methylimidazole **3b** exhibited better activities against *B. yeast* (MIC = 16 μg/mL) and *A. flavus* (MIC = 32 μg/mL) than reference fluconazole. Noticeably, all prepared compounds exhibited better efficacy than fluconazole against *A. flavus*. The results indicated that the introduction of imidazoles into 12-position of berberine can remarkably improve the bioactivity against tested microbial strains.

In view of above discussion, the antimicrobial efficacies should be closely related to imidazole ring to some extent. For this serial compounds, imidazolyl moieties contributed to the antibacterial activities in the order of unsubstituted imidazolyl > 2-methylimidazolyl > 4-methylimidazolyl > 2-ethylimidazolyl > 2-propylimidazolyl > 2-butylimidazolyl > 2,4-dimethylimidazolyl > 2-ethyl-4-methylimidazolyl > 2-undecylimidazolyl > 2-heptadecyl- imidazolyl.

Table 2 The molecular electrostatic potential (MEP) surfaces of some target compounds.

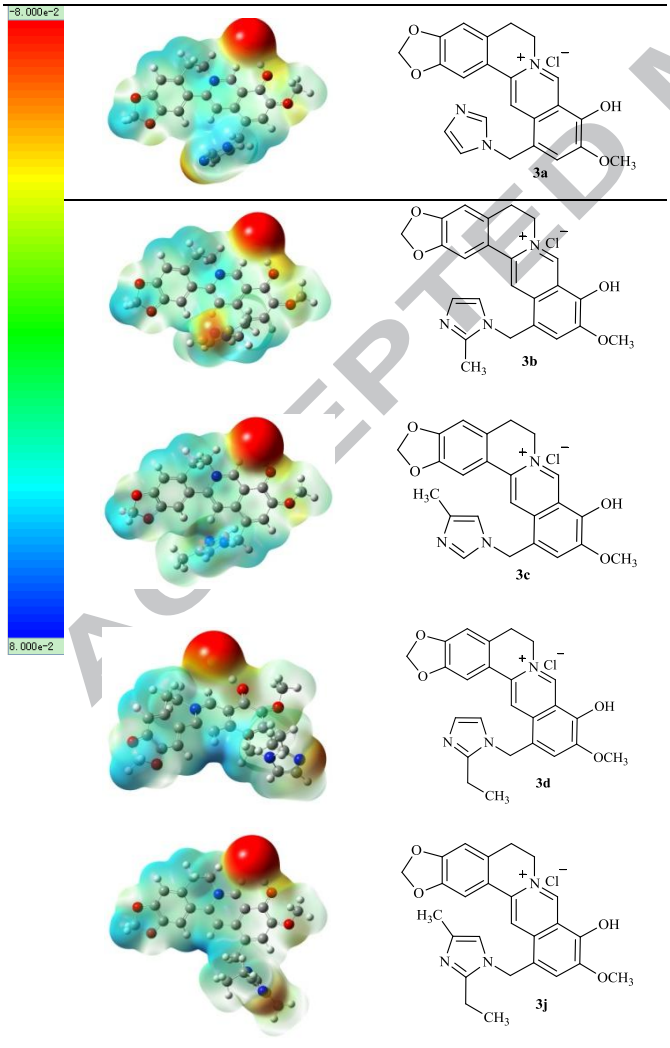

The lipid/water partition of drugs played an important role in exerting bioactivities by influencing the transportation, distribution, metabolism and secretion in organisms.[10] The calculated lipid/water partition coefficients (ClogP) of all prepared compounds by ChemDraw Ultra 10.0 were shown in Table 1. The ClogP values have been widely employed to predict transportation and bioactivities of drugs and it was revealed that compounds with lower values of ClogP exhibited more efficient antimicrobial activities. The berberine-based imidazoles **3a–c** showed lower ClogP values in contrast to its precursor berberine meaning that the newly synthesized compounds possessed more reasonable water solubility, which was favorable for them to permeate through biological membrane and to be delivered to the binding sites.

The molecular electrostatic potential (MEP) surface gives an indication of the charged surface area, an idea of the hydrophilicity of the compounds and the orientation of drug candidate for their activity.[11] Therefore, MEP maps are generated to investigate the key structural features for the target compounds such as steric, electrostatic interactions, hydrogen donor/acceptor properties and lipophilicity. Table 2 shows a comparison of the molecular electrostatic potential surfaces, which are generated for a selection of relevant studied compounds at the DFT-B3LYP level of theory for the neutral state. As shown in Table 2, the MEP surface of the berberine-based imidazoles, one electronegative area can be observed at the imidazole ring and the substituent at 2- or 4-position of imidazole ring can influence the electronegative site. In compound **3a**, the nitrogen atom in 3-position of imidazole is more electronically available with the lone pair, which probably orient toward the outer part of the molecule and therefore more accessible to interact with a variety of enzymes and receptors in biological system. However in the alkylimidazole substituted analogues such as compounds **3c** and **3j**, the nitrogen lone pair is only partially available. Owing to steric hindrance, this lone pair is buried in the structure and unavailable for interaction with solvents or other biomolecules. Therefore, the result showed that the 12-imidazolyl substituted berberine possessed larger conjugated system and electron rich properties than berberine and the substituent on imidazole had unfavorable effects on biological activities.

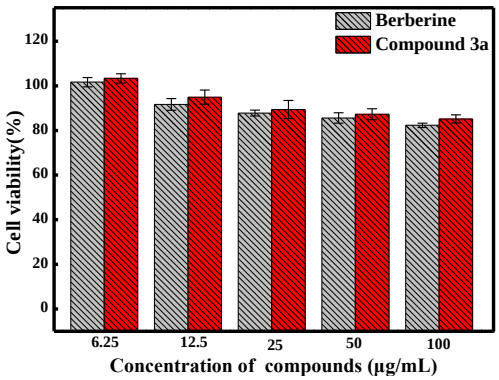

Figure 2. Cytotoxic assay of target compound **3a** and berberine on HepG2 tested by MTT methodology. Each data bar represents an average of three parallels, and error bars indicate one standard deviation from the mean.

The most bioactive compound **3a** was further examined for cytotoxic properties on HepG2 lines using the colorimetric cell proliferation MTT assay. Berberine was selected as a positive control. Cytotoxic results showed that the cell viability of compound **3a** against HepG2 cells was at least more than 87% within concentration of 100 μg/mL. Compound **3a** did not affect the cell viability of HepG2 within the MIC value. Overall, the

cell viability of compound **3a** was higher than berberine in the concentrations of 6.25, 12.5, 25, 50 and 100 μg/mL, which indicated that the novel compound showed lower cell toxicity than its precursor berberine.

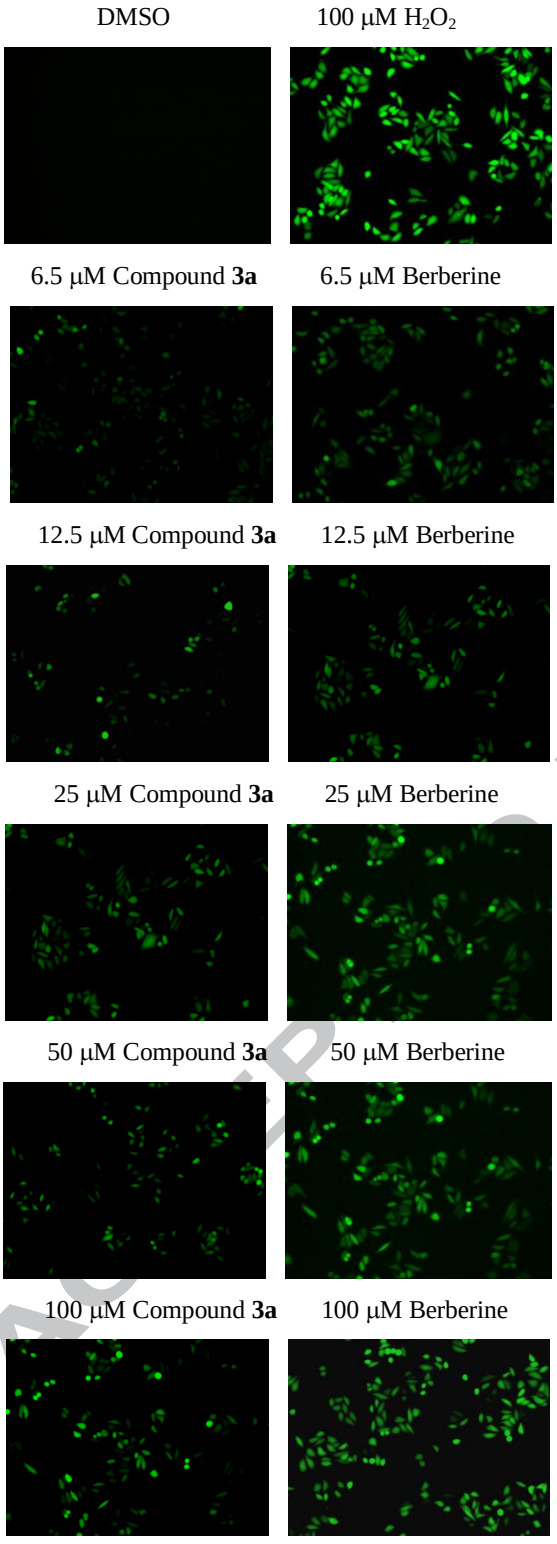

Figure 3. Compound **3a** and berberine-induced ROS formation in HepG2 cells and H_2O_2 as positive control.

The relation between antimicrobial mechanism and cell toxicity has not been fully elucidated, but it is thought to involve the photo-excitation of endogenous porphyrin molecules, a process which generates reactive oxygen species (ROS).[12] The excessive ROS could cause cellular injury, thus led to cell death and DNA damage. ROS level was investigated using DCFH-DA as a fluorescence probe and imaged by fluorescence microscope. As shown in Figure 3, target compound **3a** showed lower ROS generation than berberine at concentration of 6.25, 12.5, 25, 50 and 100 μM, respectively. Therefore, the newly synthesized compound **3a** exhibited better safety profile than clinically used berberine by down regulating ROS generation.

DNA is a significant information molecule encoding genetic instructions, which has been regarded as an important target for studies of bioactive molecules like antimicrobial drugs.[13] The interactive studies of compound **3a** with calf thymus DNA on molecular level were carried out *in vitro* by UV–vis method. With a fixed concentration of DNA, UV–vis absorption spectra were recorded with the increasing amount of compound **3a**. As shown in Figure 5, the UV–vis spectra showed that the maximum absorption peak of DNA at 260 nm exhibited proportional increase and slight red shift with the increasing concentration of compound **3a**. Meanwhile, the phenomenon indicated that the measured value of **3a**–DNA complex was a little greater than the absorption value of the simply sum of free DNA and free compound **3a**. This suggested a conformational change in the DNA duplex. This change is characteristic of non-covalent interactions between the complexes and DNA resulting in some uncoiling of the DNA helix and the exposure of some previously embedded DNA bases. The observed spectral effects can be explained by the electrostatic interaction of the complexes with DNA.

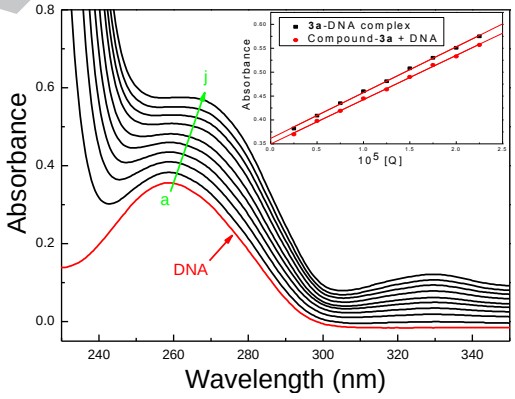

Figure 4. UV absorption spectra of DNA with different concentrations of compound **3a** (pH = 7.4, T= 303 K). Inset: comparison of absorption at 260 nm between the **3a**–DNA complex and the sum values of free DNA and free compound **3a**. c(DNA) = 5.27×10^{-5} mol/L, and c(compound **3a**) = 0–2.25×10^{-5} mol/L for curves a–j respectively at increment 0.25×10^{-5} mol/L.

Based on variations in the absorption spectra of DNA upon binding to **3a**, equation (1) can be utilized to calculate the binding constant (K)

$$\frac{A^0}{A-A^0} = \frac{\xi_C}{\xi_{D-C}-\xi_C} + \frac{\xi_C}{\xi_{D-C}-\xi_C} \times \frac{1}{K[Q]} \quad (1)$$

A^0 and A represent the absorbance of DNA in the absence and presence of compound **3a** at 260 nm, ξ_C and $\xi_{D\text{-}C}$ are the absorption coefficients of compound **3a** and **3a**–DNA complex respectively, [Q] is the concentration of compound **3a**. The plot of $A^0/(A\text{-}A^0)$ versus 1/[compound **3a**] is constructed by using the absorption titration data and linear fitting (Fig. 5), yielding the binding constant, K = 5.22×10^3 L/mol, R = 0.99994, SD = 0.04258 (R is the correlation coefficient, and SD is standard deviation)

It was apparent that the absorption peak of the Neutral Red (NR) at around 460 nm displayed gradual decrease with the increasing concentration of DNA, and a new band at around 530 nm developed. This was attributed to the formation of the new DNA–NR complex. An isosbestic point at about 504 nm

provided evidence of DNA–NR complex formation. To further understand the interaction between compound **3a** and DNA, the absorption spectra of competitive interaction of compound **3a** were investigated. NR is a planar phenazine dye, which is structurally similar to other planar dyes like thiazines and xanthenes with higher stability, lower toxicity and more convenient application. In recent years, it has been demonstrated that the binding of NR with DNA is an intercalation binding.[14] Therefore, NR was used as a spectral probe to investigate the binding mode of **3a** with DNA in this work. The absorption spectra of the NR dye upon the addition of DNA (Supplementary data: Fig. S1) revealed that the absorption peak of the NR at around 460 nm exhibited gradual decrease with the increasing concentration of DNA, and a new band at around 530 nm developed. This was attributed to the formation of the new DNA–NR complex.

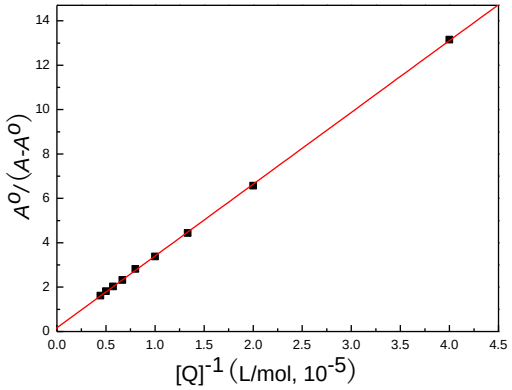

Figure 5. The plot of $A^o/(A-A^o)$ versus 1/[compound **3a**].

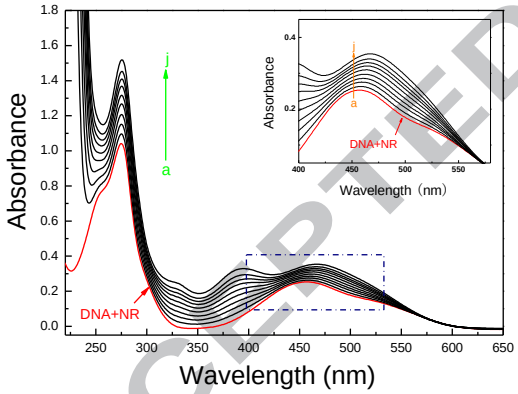

Figure 6. UV absorption spectra of the competitive reaction between **3a** and neutral red with DNA. c(DNA) = 4.11×10^{-5} mol/L, c(NR) = 2×10^{-5} mol/L, and c(compound **3a**) = 0–4.5×10^{-5} mol/L for curves *a*–*j* respectively at increment 0.5×10^{-5}. Inset: Absorption spectra of the system with the increasing concentration of **3a** in the wavelength range of 350–600 nm absorption spectra of competitive reaction between compound **3a** and NR with DNA.

As shown in Figure 6, the competitive binding between NR and **3a** with DNA was observed in the absorption spectra. With the increasing concentration of compound **3a**, an apparent intensity increase was observed around 460 nm. Compared with the absorption around 460 nm of free NR in the presence of the increasing concentrations of DNA (Fig. 6), the absorbance at the same wavelength exhibited a reverse process (inset of Fig. 6). The results suggested that compound **3a** intercalated into the double helix of DNA by substituting for NR in the DNA–NR complex. In addition, increase of absorbance at 276 nm provided evidence for intercalation of compound **3a** into DNA.

To rationalize the observed antibacterial activity and understand the possible mechanism of the target imidazolyl berberine, a flexible ligand receptor docking investigation was undertaken. The crystal structure data (topoisomerase IB–DNA complex, PDB code: 3m4a) were obtained from the Protein Data Bank, which was a representative target to investigate the antibacterial mechanism of berberines. Target compound **3a** was selected to dock onto the topoisomerase IB–DNA complex.

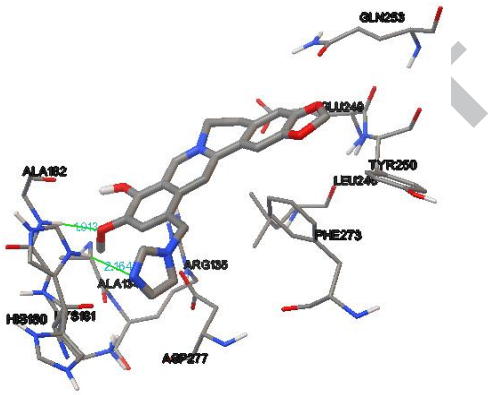

Figure 7. Three-dimensional conformation of compound **3a** docked in bacterial topoisomerase IB–DNA complex.

The docking mode with the lowest binding free energy (-7.00 kJ/mol) is shown in Figure 7 (Supplementary data: Fig. S2 and S3). The docking result of compound **3a** with topoisomerase IB–DNA complex might rationalize the possible antibacterial mechanism. The methoxyl group in the 9-position of berberine was in close proximity to the residue ALA-182 through hydrogen bonds with distance of 1.913 Å. Moreover, this molecule **3a** could also form hydrogen bonds with HIS-180 of topoisomerase IB–DNA complex with distance of 2.164 Å through the nitrogen atom of imidazolyl moiety, which indicated the necessity of imidazole group for the increased bioactivity. In addition, electrostatic interactions exist between the aromatic ring of compound **3a** and GLN-253, GLU-249, TYR-250, LEU-246, PHE-273, ASP-277, PHE-273, LYS-181, ALA-134 in DNA topoisomerase IB. These hydrogen bonds might be beneficial to stabilize the compound–DNA–enzyme complex, which might be the important reason that compound **3a** displayed strong inhibitory efficacy against tested strains.

In conclusion, a novel series of berberine-derived imidazole compounds were successfully synthesized by a convenient and efficient procedure. Their structures were confirmed by ^{1}H NMR, ^{13}C NMR, MS, IR and HRMS spectra. The *in vitro* antimicrobial evaluation revealed that most of the synthesized compounds exhibited good bioactivities against the tested Gram-positive and Gram-negative bacteria. Especially compound **3a** against *E. typhosa*, *B. subtilis* and MRSA with MIC values of 1–32 μg/mL was superior to reference drugs. Structure-activity relationship suggested that imidazolyl group was important for exerting antibacterial and antifungal efficacy and the introduction of bulky alkyl substituted imidazole fragment into C-12 position of berberine would decrease the antibacterial activity. The cell toxicity and ROS generation assay displayed that compound **3a** showed low cytotoxicity by down regulating ROS generation. The interactive investigations revealed that compound **3a** could effectively intercalate into calf thymus DNA to form **3a**–DNA complex which might further block DNA replication to exert the powerfully antimicrobial activities. Molecular docking indicated that compound **3a** could bind with DNA topoisomerase IB through hydrogen bonds and electrostatic interactions. Further research, including the introduction of other azoles (*eg*. aminoimidazole, triazole) into C-12 position of berberine as well as *in vivo* biological studies

are currently in progress, and all these will be discussed in the future paper.

Acknowledgments

This work was partially supported by National Natural Science Foundation of China [(No. 21372186), the Research Fund for International Young Scientists from International (Regional) Cooperation and Exchange Program NSFC (No. 81450110451)], the Specialized Research Fund for the Doctoral Program of Higher Education of China (SRFDP 20110182110007) and Chongqing Special Foundation for Postdoctoral Research Proposal (Xm2015031).

References and notes

1. (a) Weir, K. *Nature* **2015**, *528*, S130; (b) McKenney, P. T.; Pamer, E. G. *Cell* **2015**, *163*, 1326; (c) Escoll, P.; Mondino, S.; Rolando, M.; Buchrieser, C. *Nat. Rev. Microbiol.* **2016**, *14*, 5; (d) Peng, X. M.; Cai, G. X.; Zhou, C. H. *Curr. Top. Med. Chem.* **2013**, *13*, 1963; (e) Zhou, C. H.; Wang, Y. *Curr. Med. Chem.* **2012**, *19*, 239.
2. (a) Ni, W. J.; Ding, H. H.; Tang, L. Q. *Eur. J. Pharmacol.* **2015**, *760*, 103; (b) Bansal, Y.; Silakari, O. *Eur. J. Med. Chem.* **2014**, *76*, 31; (c) Kumar, A.; Ekavali, C. K.; Mukherjee, M.; Pottabathini, R.; Dhull, D. K. *Eur. J. Pharmacol.* **2015**, *761*, 288; (d) Kaboli, P. J.; Rahmat, A.; Ismail, P.; Ling, K. H. *Eur. J. Pharmacol.* **2014**, *740*, 584.
3. Tillhon, M.; Ortiz, L. M. G.; Lombardi, P.; Scovassi, A. I. *Biochem. Pharmacol.* **2012**, *84*, 1260.
4. (a) Domadia, P. N.; Bhunia, A.; Sivaraman, J.; Swarup, S.; Dasgupta, D. *Biochemistry* **2008**, *47*, 3225; (b) Ball, A. R.; Casadei, G.; Samosorn, S.; Bremner, J. B.; Ausubel, F. M.; Moy, T. I.; Lewis, K. *ACS Chem. Biol.* **2006**, *1*, 594; (c) Xu, Y.; Wang, Y.; Yan, L.; Liang, R. M.; Dai, B. D.; Tang, R. J.; Gao, P. H.; Jiang, Y. Y. *J. Proteome Res.* **2009**, *8*, 5296; (d) Domadia, P. N.; Bhunia A.; Sivaraman, J.; Swarup, S.; Dasgupta, D. *Biochemistry* **2008**, *47*, 3225.
5. (a) Zhang, L.; Chang, J. J.; Zhang, S. L.; Damu, G. L. V.; Geng, R. X.; Zhou, C. H. *Bioorg. Med. Chem.* **2013**, *21*, 4158; (b) Zhang, S. L.; Chang, J. J.; Damu, G. L. V.; Fang, B.; Zhou, X. D.; Geng, R. X.; Zhou, C. H. *Bioorg. Med. Chem. Lett.* **2013**, *23*, 1008; (c) Zhang, S. L.; Chang, J. J.; Damu, G. L. V.; Geng, R. X.; Zhou, C. H. *Med. Chem. Comm.* **2013**, *4*, 839.
6. (a) Li, R.; Wu, J.; He, Y.; Hai, L.; Wu, Y. *Bioorg. Med. Chem. Lett.* **2014**, *24*, 1762; (b) Iwasa, K.; Lee, D. U.; Kang, S. I.; Wiegrebe, W. *J. Nat. Prod.* **1998**, *61*, 1150.
7. (a) Zhang, L.; Peng, X. M.; Damu, G. L. V.; Geng, R. X.; Zhou, C. H. *Med. Res. Rev.* **2014**, *34*, 340; (b) Zhang, L.; Kumar, K. V.; Rasheed, S.; Zhang, S. L.; Geng, R. X.; Zhou, C. H. *MedChemCommun* **2015**, *6*, 1405; (c) Peng, X. M.; Damu, G. L. V.; Zhou, C. H. *Curr. Pharm. Des.* **2013**, *19*, 3884; (d) Zhang, L.; Addla, D.; Ponmani, J.; Wang, A.; Xie, D.; Wang, Y. N.; Zhang, S. L.; Geng, R. X.; Cai, G. X.; Li, S.; Zhou, C. H. *Eur. J. Med. Chem.* **2016**, *111*, 160; (e) Zhang, L.; Kumar, V. K.; Geng, R. X.; Zhou, C. H. *Bioorg. Med. Chem. Lett.* **2015**, 25, 3699; (f) Damu, G. L. V.; Cui, S. F.; Peng, X. M.; Wen, Q. M.; Cai, G. X.; Zhou, C. H. *Bioorg. Med. Chem. Lett.* **2014**, *24*, 3605.
8. Berberine hydrochloride **1** (30.0 g, 62.1 mmol) was placed in the round bottom flask and in a vacuum (20 mm Hg), stirred at 190 ^{o}C for 30 min to give the crude product, which was purified using flash silica gel column chromatography ($CHCl_3$/MeOH = 10:1) to give berberrubine **2** as red solid (25.5 g, 88.4% yield).
9. National Committee for Clinical Laboratory Standards Approved standard Document, M27-A2, Reference Method for Broth Dilution Antifungal Susceptibility Testing of Yeasts. National Committee for Clinical Laboratory Standards, Wayne, PA, 2002.
10. (a) Hunziker, D.; Wyss, P. C.; Angehrn, P.; Mueller, A.; Marty, H. P.; Halm, R.; Kellenberger, L.; Bitsch, V.; Biringer, G.; Arnold, W.; Stämpfli, A.; Schmitt-Hoffmannb, A.; Cousot, D. *Bioorg. Med. Chem.* **2004**, *12*, 3503; (b) Zhang, S. L.; Damu, G. L. V.; Zhang, L.; Geng, R. X.; Zhou, C. H. *Eur. J. Med. Chem.* **2012**, *55*, 164; (c) Rackham, M. D.; Brannigan, J. A.; Rangachari, K.; Meister, S.; Wilkinson, A. J.; Holder, A. A.; Leatherbarrow, R. J.; Tate, E. W. *J. Med. Chem.* **2014**, *57*, 2773; (d) Kügler, F.; Sihver, W.; Ermert, J.; Hübner, H.; Gmeiner, P.; Prante, O.; Coenen, H. H. *J. Med. Chem.* **2011**, *54*, 8343.
11. (a) Salas, P. F.; Herrmann, C.; Cawthray, J. F.; Nimphius, C.; Kenkel, A.; Chen, J.; de Kock, C.; Smith, P. J.; Patrick, B. O.; Adam, M. J.; Orvig, C. *J. Med. Chem.* **2013**, *56*, 1596; (b) Sharma, P.; Chhabra, S.; Rai, N.; Ghoshal, N. *J. Chem. Inf. Model.* **2007**, *47*, 1087; (c) Boström, J.; Grant, J. A.; Fjellström, O.; Thelin, A.; Gustafsson, D. *J. Med. Chem.* **2013**, 56, 3273; (d) Hirayama, T.; Okaniwa, M.; Banno, H.; Kakei, H.; Ohashi, A.; Iwai, K.; Ohori, M.; Mori, K.; Gotou, M.; Kawamoto, T.; Yokota, A.; Ishikawa, T. *J. Med. Chem.* **2015**, *58*, 8036.
12. (a) Ramakrishnan, P.; Maclean, M.; MacGregor, S. J.; Anderson, J. G.; Grant, M. H. *Toxicology in Vitro* **2016**, *33*, 54; (b) Hu, L.; Li, L.; Xu, D.; Xia, X.; Pi, R.; Xu, D.; Wang, W.; Du, H.; Song, E.; Song, Y. *Chem. Biol. Interact.* **2014**, *213*, 51; (c) Kumar, S.; Rhim, W. K.; Lim, D. K.; Nam, J. M. *ACS Nano* **2013**, *7*, 2221.
13. (a) Cui, S. F.; Ren, Y.; Zhang, S. L.; Peng, X. M.; Damu, G. L. V.; Geng, R. X.; Zhou, C. H. *Bioorg. Med. Chem. Lett.* **2013**, 23, 3267; (b) Zhang, H. Z.; Jeyakkumar, P.; Kumar, K. V.; Zhou, C. H. *New J. Chem.* **2015**, *39*, 5776; (c) Peng, L. P.; Nagarajan, S.; Rasheed, S.; Zhou, C. H. *Med. Chem. Comm.* **2015**, *6*, 222.
14. (a) Yin, B. T.; Yan, C. Y; Peng, X. M.; Zhang, S. L.; Rasheed, S.; Geng, R. X.; Zhou, C. H. *Eur. J. Med. Chem.* **2014**, *71*, 148; (b) Ni, Y.; Dua, S.; Kokot, S. *Anal. Chim. Acta* **2007**, *584*, 19; (c) Gong, H. H.; Baathulaa, K.; Lv, J. S.; Cai, G. X.; Zhou, C. H. *MedChemCommun* **2016**, DOI: 10.1039/C5MD00574D.
15. Experimental: Melting points are determined on X–6 melting point apparatus and uncorrected. IR spectra were determined on a Bio-Rad FTS-185 spectrophotometer in the range of 400–4000 cm^{-1}. ^{1}H NMR and ^{13}C NMR spectra were recorded on a Bruker AV 600 or Varian 300 spectrometer using TMS as an internal standard. Chemical shifts were reported in parts per million (ppm), the coupling constants (J) were expressed in hertz (Hz) and signals were described as singlet (s), doublet (d), triplet (t), as well as multiplet (m). The mass spectra (MS) were recorded on LCMS–2010A and the high-resolution mass spectra (HRMS) were recorded on an IonSpec FT-ICR mass spectrometer with ESI resource. All chemicals and solvents were commercially available, and used without further purification. The UV spectrum was recorded at room temperature on a TU-2450 spectrophotometer (Puxi Analytic Instrument Ltd. of Beijing, China) equipped with 1.0 cm quartz cells. The concentration of DNA in stock solution was determined by UV absorption at 260 nm using a molar absorption coefficient ξ_{260} = 6600 L mol^{-1} cm^{-1} (expressed as molarity of phosphate groups) by Bouguer–Lambert–Beer law. The purity of the DNA was checked by monitoring the ratio of the absorbance at 260 nm to that at 280 nm. The solution gave a ratio of > 1.8 at A260/A280, which indicates that DNA was sufficiently free from protein. All of the solutions were adjusted with Tris-HCl buffer solution (pH = 7.4), which was prepared by mixing and diluting Tris solution with HCl solution. All chemicals were of analytical reagent grade, and doubly distilled water was used throughout.
16. *Synthesis of 12-((1H-imidazol-1-yl)methyl)-9-hydroxy-10-methoxy-5,6-dihydro-[1,3]dioxolo[4,5-g]isoquinolino[3,2-a] isoquinolin-7-ium chloride* (**3a**)
To a solution of imidazole (340.4 mg, 5.0 mmol), formaldehyde aqueous solution (37%, 0.4 mL, 5.0 mmol) and hydrochloric acid (catalytic amount) in anhydrous n-butanol (5.0 mL) was added hydrochloride berberrubine (357.8 mg, 1.0 mmol). The resulting mixture was stirred at 110 ^{o}C for 5 h. After the reaction was completed (monitored by TLC, chloroform/methanol (10/1, V/V)), concentrated under reduced pressure to give the crude product, which was purified using silica gel column chromatography (chloroform/methanol = 20:1) to give 223.3 mg of **3a** as dark red solid. Yield: 51%; m.p.: > 250 °C; IR (KBr, cm^{-1}) ν: 3401 (OH), 3140, 3092, 3033 (Ar-H), 2962, 2930 (CH_2, CH_3) cm^{-1}; ^{1}H NMR (600 MHz, MeOD) δ 9.22 (s, 1H, 8-*H*), 7.96 (s, 1H, 13-*H*), 7.68 (s, 1H, 1-*H*), 7.45 (s, 1H, Im-*H*), 7.38 (s, 1H, 4-*H*), 7.00 (s, 1H, Im-*H*), 6.85 (s, 1H, Im-*H*), 6.76 (s, 1H, 11-*H*), 5.95 (s, 2H, OCH_2O), 5.45 (s, 2H, CH_2), 4.52–4.48 (m, 2H, 6-*H*), 3.80 (s, 3H, OCH_3), 3.05–3.01 (m, 2H, 5-*H*) ppm; ^{13}C NMR (151 MHz, MeOD) δ 164.51, 149.83, 149.39, 148.22, 146.53, 136.88, 135.31, 130.07, 129.80, 127.81, 124.37, 121.44, 120.49, 119.19, 113.69, 110.70, 107.87, 104.70, 101.93, 55.50, 54.04, 46.82, 27.49 ppm; HRMS (ESI) calcd. for $C_{23}H_{20}ClN_3O_4$ $[M\text{-}Cl]^+$, 402.1448; found, 402.1447.

Graphical Abstract

Discovery of novel berberine imidazoles as safe antimicrobial agents by down regulating ROS generation

Leave this area blank for abstract info.

Si-Qi Wen, Ponmani Jeyakkumar[†], Srinivasa Rao Avula[‡], Ling Zhang, Cheng-He Zhou[*]

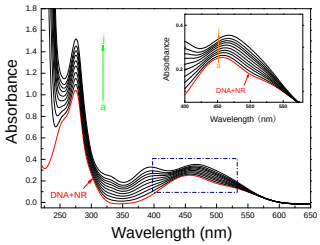

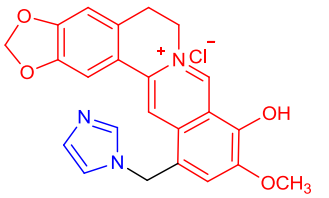

MIC = 1 μg/mL (*E. typhosa*)